Differential phase technique with the Keck Interferometer

Rachel L. Akeson, Mark R. Swain, M. Mark Colavita

Rachel L. Akeson, Mark R. Swain, M. Mark Colavita, "Differential phase technique with the Keck Interferometer," Proc. SPIE 4006, Interferometry in Optical Astronomy, (5 July 2000); doi: 10.1117/12.390222

SPIE.

Event: Astronomical Telescopes and Instrumentation, 2000, Munich, Germany

Differential phase technique with the Keck Interferometer

Rachel L. Akeson[a], Mark R. Swain[b] and M. Mark Colavita[b]

[a] Infrared Processing and Analysis Center, California Institute of Technology, Pasadena, CA, 91125 USA

[b] Jet Propulsion Laboratory, California Institute of Technology, 4800 Oak Grove Drive, Pasadena, CA, 91109 USA

ABSTRACT

We present the motivation and development of the novel "differential phase" technique being developed for the Keck Interferometer with the goal of detecting faint companions near a bright source. The differential phase technique uses simultaneous phase measurements at several infrared wavelengths to detect the astrophysical signature produced by a chromatic, asymmetric brightness distribution. We discuss the origin of the differential phase signature and present results of test observations taken at the Palomar Testbed Interferometer. One important test result is the larger than expected effect of water vapor turbulence on these multi-wavelength observations due to the infrared dispersion of water. In order to reach the design goal of 0.1 milliradians, the phase noise caused by both temperature and water vapor fluctuations in the atmosphere must be corrected, and we discuss several ways to achieve this.

By combining the 10 meter Keck telescopes, this technique will enable measurement and characterization of some of the known extra solar planets, such as the companion to 51 Peg. A large intensity difference exists between the stellar primary and the planetary companion, and the differential phase technique converts the problem of intensity dynamic range to one of phase dynamic range. In addition to enabling the direct detection of extra solar planets, this technique is applicable to other science objectives.

Keywords: infrared interferometry, atmospheric dispersion

1. INTRODUCTION

Direct detection of extrasolar planets is challenging due to the high intensity ratio and small angular separation between the planet and the star. For example, the planet/star flux ratio of a Jupiter-size planet orbiting 0.05 AU from a solar-type star is $\sim 10^{-8}$ in the optical and $\sim 10^{-4}$ at 2 μm. While the planet in isolation could easily be detected at this flux level, the nearby star makes this detection a problem of intensity dynamic range and spatial resolution. At a distance of 20 pc, the angular separation of this planetary companion is $\sim$2.5 milliarcseconds, smaller than the diffraction limit of a single Keck 10-m telescope. Interferometric techniques can provide both the necessary sensitivity and spatial resolution to study extrasolar planets in the infrared.

2. DIFFERENTIAL PHASE TECHNIQUE

The Palomar Testbed Interferometer (PTI)[1] and the Keck Interferometer[2] are direct detection infrared interferometers with active fringe tracking. The fringe amplitude and phase are measured by scanning the delay line over a delay of one wavelength and measuring the flux in each of four time bins, designated A, B, C, and D (see Ref. 3 for more details on this technique). Neglecting the bias term, the squared visibility and phase are given by

$$V^2 = \frac{\pi}{2} \frac{\langle (A-C)^2 + (B-D)^2 \rangle}{\langle A+B+C+D \rangle^2}$$

$$\phi = \tan^{-1} \frac{B-D}{A-C}.$$

Further author information: (Send correspondence to RLA: email akeson@huey.jpl.nasa.gov)

In *Interferometry in Optical Astronomy*, Pierre J. Léna, Andreas Quirrenbach, Editors,
Proceedings of SPIE Vol. 4006 (2000) • 0277-786X/00/$15.00

2.1. Differential phase

For differential phase observations, the presence of a faint companion is determined using measurement of the fringe phase simultaneously at several wavelengths. A phase difference as a function of wavelength is produced by sources with different spectral energy distributions, as the source amplitudes will contribute different fractions to the measured fringe phase at different wavelengths. In the narrow band limit, the fringe from the primary is given by

$$\mathcal{A}_p \cos(kx)$$

where $k = 2\pi/\lambda$ and x is the delay. The secondary source fringe is given by

$$\mathcal{A}_s \cos[k(x+\delta)],$$

where δ is the separation of the two sources on the sky as measured in delay space and is a function of the baseline and $\vec{ds}$, the separation on the sky, i.e., $\delta = \vec{ds} \cdot \vec{B}$. Both the fringe amplitude $\mathcal{A}_p$ and $\mathcal{A}_s$, as well as k, will depend on the wavelength band. The relative contribution of the primary and secondary to the flux for a particular measurement bin, A, B, C, D, is given by

$$\mathrm{A}_{\lambda_1} = \int_0^{\lambda_1/4} \mathcal{A}_p \cos[k_1 x]\, dx + \int_0^{\lambda_1/4} \mathcal{A}_s \cos[k_1 (x+\delta)]\, dx$$

$$\mathrm{B}_{\lambda_1} = \int_{\lambda_1/4}^{\lambda_1/2} \mathcal{A}_p \cos[k_1 x]\, dx + \int_{\lambda_1/4}^{\lambda_1/2} \mathcal{A}_s \cos[k_1 (x+\delta)]\, dx$$

and so on. Once the source flux densities and separation vector are specified, the phase at each wavelength and the differential phase can be easily computed from these integrals. As the interferometer tracks a source across the sky, the projected baseline will evolve in time. Thus, the differential phase for a given source will be a function of hour angle (Figure 1).

As the maximum differential phase effect is approximately equal to the relative source fluxes, it is essential to make very precise phase measurements. As the same beam path is used for all wavelengths, and by measuring the phases simultaneously, all common-mode achoromatic systematic effects will be removed from the observed differential phase observable.

One complication for differential phase observations is the wavelength dependence of the atmospheric dispersion. If this effect is not corrected, the fringe packets at different wavelengths will not be at the same location in delay space. An atmospheric dispersion compensator (ADC) is necessary to compensate the dispersive phase delay between wavelengths, allowing the fringe tracker to make simultaneous phase measurements.

3. DIFFERENTIAL PHASE AT PTI

3.1. Demonstration observations

As part of the development effort for differential phase, test observations were made at PTI. A well-studied binary source,[4] ι Peg (HD 210027) was specifically chosen to give a large differential phase signature, which is produced by a large color difference between the components and a binary separation of at least one fringe spacing. During the 1997 and 1998 observing seasons, ι Peg was observed and its orbital parameters were derived as part of the binary orbit program at PTI.[4]

A differential phase metric can be constructed from any two channel phases. Widely separated wavelengths tend to have larger differential phase signatures, although this depends on the details of the source spectra. For the PTI data, we have used the group delay estimate as a differential phase metric and concentrated on observations within the K band. As part of the normal observing procedure, the real-time system at PTI calculates a group delay estimate every 0.5 seconds. This estimate uses a complex Fourier transform of the channel quadratures and is analogous to a straight line fit to the channel phases.[1] The fringe tracker, which tracks the broadband fringe phase, uses the group delay to keep the track point on the central fringe. If the measurement has sufficient signal-to-noise, a group delay value outside the range $\pm\lambda/2$ will cause the fringe tracker to hop one fringe. Due to compensation of the

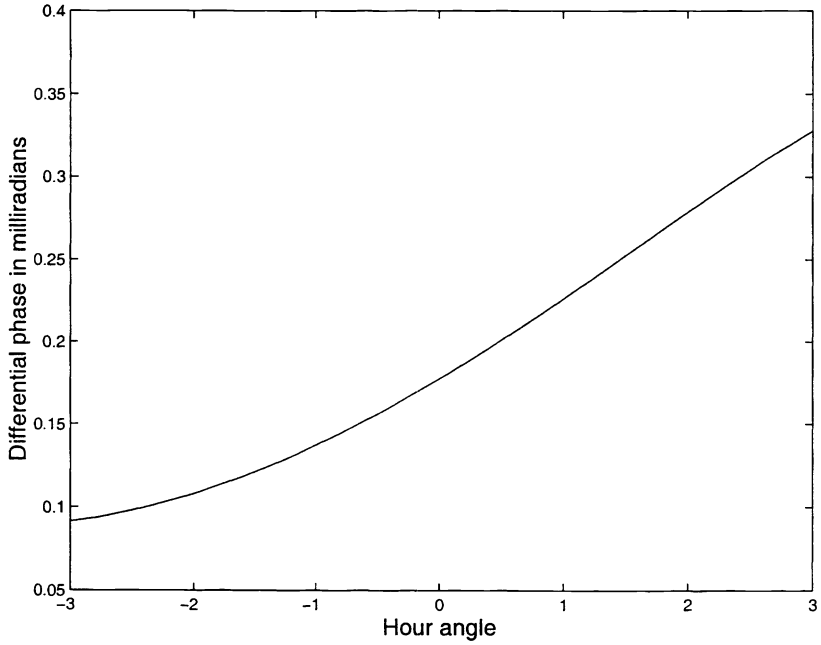

Figure 1. Predicted differential phase between the K and L bands as a function of hour angle for a star and planet binary system like 51 Peg (see section 4.1) as observed by the Keck-Keck baseline.

vacuum delay with a dispersive air path, the fringe phase and the fringe envelope have slightly different velocities, which correspond to a group delay change of one fringe (2.2 microns) for every ~4 meters of change in delay. We will refer to this as the sidereal signature. Before a source can be evaluated for a differential phase signature, the sidereal signature must be measured and removed. The group delay signature is a function of delay and has two parameters: a slope of group delay over delay and an offset in delay. Once this signature and any instrumental effects are removed, any group delay value significantly different from 0 should be due to source characteristics.

An example of group delay data showing a clear sidereal signature is given in Figure 2. The data in the top panel are from night 99186, which had low group delay noise, while the bottom panel is data from the same source from night 99169, where the group delay is more noisy. As discussed in Section 3.2, our current understanding of the infrared dispersion due to water suggests that the group delay noise is dominated by water vapor fluctuations in the atmosphere, the magnitude of which vary greatly from night to night at PTI.

ι Peg was observed for over 2 hours in good weather conditions on night 99304. On this night, only 1 calibrator, HD 209761, was observed. The sidereal signature measured on the calibrator using the above procedure produced a best-fit slope (group delay/delay) of -5.85×10^{-7} μm/μm and an offset of -2.2×10^{6} μm. The residual rms after removing this sidereal signature is 0.42 μm, but the residual time series shows remaining structure within each 130 scan, consistent with water vapor fluctuations, and some low frequency structure over the 2 hour time interval. This low frequency structure was removed by averaging the data points within each scan and interpolating in time. The low frequency structure may be caused by instrumental effects or by long term changes in the water column. The sidereal slope and the scan average were both subtracted from the source group delay (Figure 3). The source group delay is clearly offset from zero and is consistent with the predicted differential phase.

The differential phase for ι Peg is predicted as described in Section 2.1 using the orbital parameters from Ref. 4 and the PTI baseline. Blackbody spectra are used for both of the components with spectral types of F5V for the primary and G8V for the secondary, with effective temperatures of 6440 and 5570 K, respectively. The flux of the secondary is scaled to match the measured intensity ratio in the K band. The distance to the system is 11.5 pc.

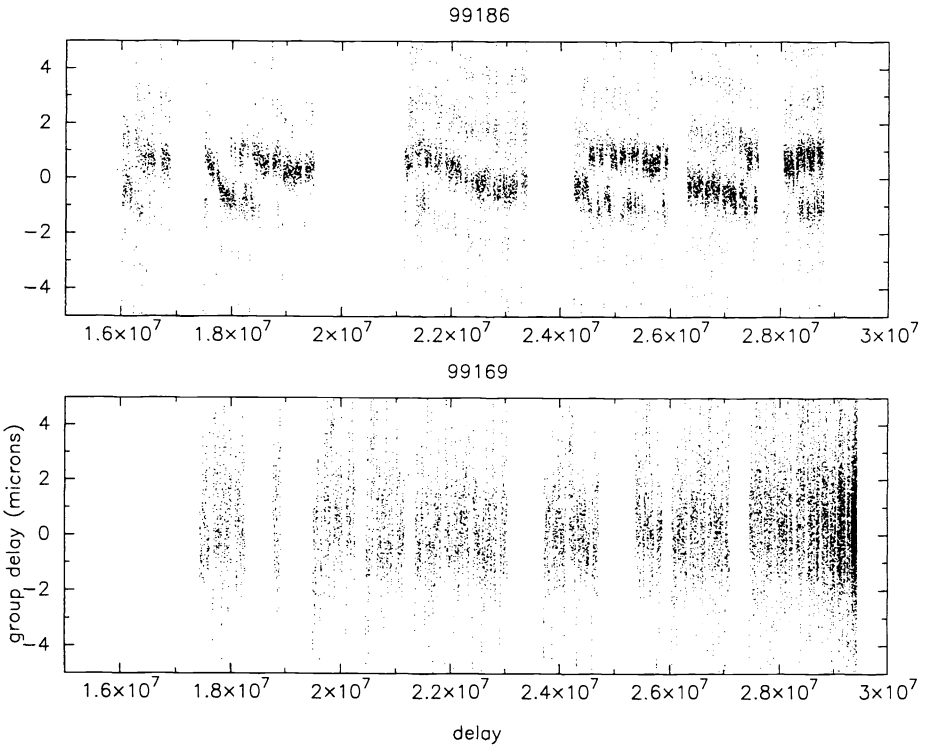

Figure 2. Measured group delay as a function of total delay for two nights at PTI. The top panel (night 99186) shows a night with low group delay noise where the sidereal signature is apparent. The bottom panel (night 99169) shows observations of the same source on a second night where the group delay noise is much higher. Each point represents 0.5 seconds of data.

3.2. Atmospheric limitations

Dispersion in the dry atmosphere above the interferometer results in leakage of the systematic delay, causing the sidereal signature discussed above, as well as the seeing, into the group delay. However, the seeing term should be much smaller than the systematic term, and doesn't explain the excess noise seen in Fig. 2. While the effects of water vapor on seeing are typically ignored for astronomical observations in the visible and near-infrared bands, our hypothesis was that we were seeing an effect attributable to atmospheric water vapor via a strongly dispersive refractive index. This would not be expected from simply extrapolating the traditional optical formulae[5] to the near-infrared. However, a recent calculation of the water vapor refractive index across the K band (by the same group, and with the same approach, as Ref. 6, which calculated the index at 10 μm and at a few points near 3.5 μm), leads to a water vapor refractive index with 20 times more dispersion than an extrapolation of the optical formulae. These analytic results are consistent with water vapor index measurements performed at PTI, and suggests that leakage to the differential phase via a highly dispersive water vapor refractive index is indeed responsible for the excess noise seen in the PTI data. For the atmospheric conditions corresponding to a good night on Mauna Kea, the water vapor seeing component of the differential phase metric is $\sim$1000 times larger than the astrophysical signature and integration times of 1 hour reduce the seeing contribution by a factor of 25.

We have investigated several techniques to mitigate the effects of atmospheric water vapor. One approach is to use the dual-star feed to simultaneously observe a nearby (separation less than a few arcmin) calibrator source, which is assumed to have no intrinsic differential phase signature, to measure the atmospheric and instrument group delay fluctuations and apply this correction to the source. This method is the most direct; however, not all of the target sources have suitable calibrators. The differential water vapor can also be estimated using the intensity fluctuations in the water line between the H and K bands. For the total water columns typical for good night at Mauna Kea, this

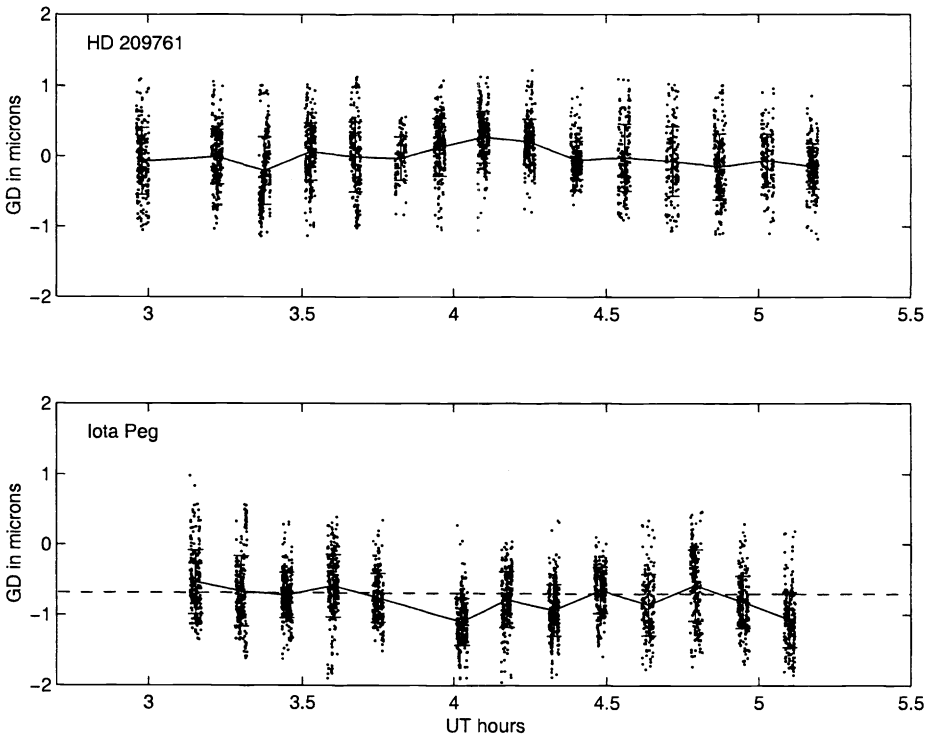

Figure 3. 99304 data. Top: HD 209761 data with sidereal fit removed (points) and 4th order polynomial fit (line). Bottom: ι Peg (HD 210027) data with sidereal and scan averaged fit from calibrator removed (points), average of ι Peg by scan (solid line) and predicted differential phase (dashed line). Each point represents 0.5 seconds of data.

line is not saturated and small changes in the total column result in small changes in the transmission. For these bright target sources ($K_{mag} \sim 5$), this method yields a factor of 10 improvement, although there may be difficulty transferring the data to the differential phase metric. Probably the best approach is to take measurements at several different wavelengths and to use the different wavelength dependencies of the water vapor and the source differential phase to separate the astronomical and atmospheric effects. If the refractivities of the dry atmosphere and the water and the shape of the differential phase signature as a function of wavelength are known and are not degenerate, the magnitude of the differential phase can be determined from phase measurements at several wavelengths using matrix inversion or least squares methods.

4. DIFFERENTIAL PHASE WITH THE KECK INTERFEROMETER

4.1. Candidate sources and predicted signatures

The companions to nearby stars discovered through radial velocity searches[7] are the best candidates for differential phase observations. As warmer planets will have a larger flux relative to the stellar flux, and therefore a larger differential phase, planets with orbital radii less than 0.1 AU are the best targets for the Keck Interferometer (Table 1).

Observations of planet candidates found with the radial velocity technique yield the planet mass times the sine of the inclination and the orbit. Predictions for the composition and temperature of these planets come from modeling, extrapolation from our own solar system, and recent spectral data from cool brown dwarfs such as Gliese 229B. To investigate the range of differential phase signatures possible from the close-in systems (radii < 0.1 AU), we have examined models from Ref. 8–10. Models of isolated planets and brown dwarfs such as the work of Refs. 11,12 are not applicable for the close-in planets due to the intense stellar radiation. A close-in planet will have a different

Star Name	M sin i M_J	Period days	Semi-major axis AU	mas	Eccentricity	T_{star} K	T_{planet} K
HD 187123	0.52	3.1	0.042	0.9	0.00	5830	1290
τ Bootis	3.64	3.3	0.042	2.7	0.00	6600	1540
HD 209458	0.69	3.5	0.045	0.001	0.0	6000	1300
HD 75289	0.42	3.5	0.046	0.016	0.053	6030	1350
51 Pegasi	0.44	4.2	0.051	3.3	0.01	5750	1230
υ Andromedae	0.63	4.6	0.053	3.9	0.03	6200	1480
HD 217107	1.28	7.1	0.07	3.5	0.14	5570	980

Table 1. Masses and orbital characteristics of the close-in candidate extrasolar planet systems. The planet temperatures are calculated for an albedo of 0.25.

atmospheric temperature-pressure profile as compared to an isolated planet with the same effective temperature. For close-in planets, light reflected from the primary will dominate the planetary spectrum at optical wavelengths, but the reflected component is not substantial at near-infrared and longer wavelengths.[9,10]

The three groups[8–10] have all produced models for 51 Peg, and we have used these models in estimating the differential phase signature. Although all groups find effective temperatures in the range 1200-1300 K, the predicted infrared spectra vary from a nearly featureless, almost blackbody spectrum[8] to strong departures from blackbody due to molecular lines.[10,9] These three spectra, given in terms of planet/stellar flux ratio are shown in Figure 4. Using these spectra, the predicted differential signature between the H and K bands is roughly 0.1 milliradians. Extending the measurements to the L or M bands increases the signature to ~0.3 milliradians due to the higher planet/stellar flux ratio at these wavelengths.

4.2. Observations and systematics

To measure the differential phase at the levels predicted above, minimization of the atmospheric and instrumental terms is essential. As discussed in Section 3.2, differential phase measurements must account for dispersion in both the dry and wet atmospheric components to yield an observable which is independent of the seeing. Contributions from instrument systematics are important at the level of tenths of milliradians. In particular, the delay line stroke, fringe wavelength and beam walk must be well calibrated.

ACKNOWLEDGMENTS

This work was performed at the Infrared Processing and Analysis Center, California Institute of Technology and the Jet Propulsion Laboratory, California Institute of Technology, under a contract with the National Aeronautics and Space Administration. Interferometer data were obtained at Palomar Observatory using the NASA Palomar Testbed Interferometer supported by NASA contracts to the Jet Propulsion Laboratory and observations at PTI are made possible through the efforts of the PTI Collaboration (`http://huey.jpl.nasa.gov/palomar/ptimembers.html`). Funding for the Keck Interferometer provided by the National Aeronautics and Space Administration.

REFERENCES

1. M. M. Colavita et al, "The Palomar Testbed Interferometer," *Ap. J.* **510**, pp. 505–521, 1999.
2. M. M. Colavita and P. L. Wizinowich, "Keck interferometer: progress report," in *Interferometery in Optical Astronomy*, vol. (this proceedings), 2000.
3. M. M. Colavita, "Fringe visibility estimators for the Palomar Testbed Interferometer," *PASP* **111**, pp. 111–117, 1999.
4. A. F. Boden, C. D. Koresko, G. T. van Belle, M. M. Colavita, P. J. Dumont, J. Gubler, S. R. Kulkarni, B. F. Lane, D. Mobley, M. Shao, J. K. Wallace, The PTI Collaboration, and G. W. Henry, "The visual orbit of iota Pegasi," *Ap. J.* **515**, pp. 356–364, 1999.
5. J. Owens, "Optical refractive index of air: dependence on pressure, temperature and composition," *Appl. Opt.* **6**, pp. 51–59, 1967.

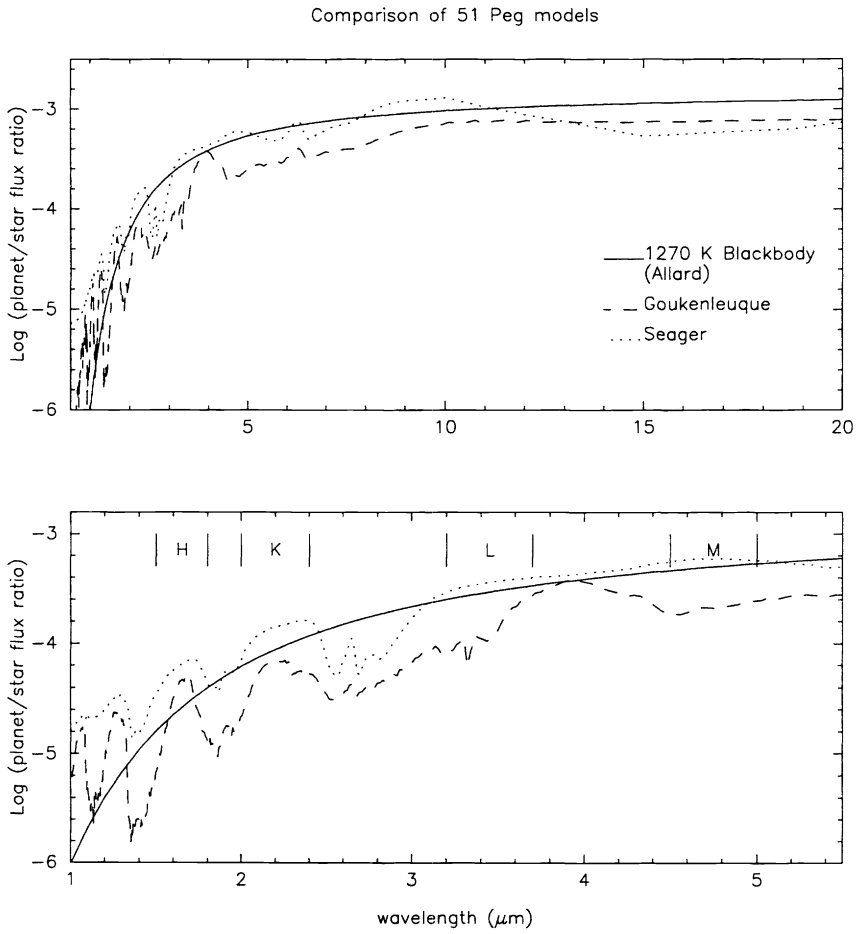

Figure 4. Ratio of planet to stellar flux for three models of the 51 Peg system. The spectra are taken from Ref. 8-10.

6. R. J. Hill and R. S. Lawrence, "Refractive index of water vapor in infrared windows," *Infrared Phys.* **26**, pp. 371–376, 1986.
7. G. W. Marcy and R. P. Butler, "Detection of extrasolar giant planets," *ARAA* **36**, pp. 57–97, 1998.
8. F. Allard, "Models, atmospheres, and spectra of brown dwarfs to giant planets," in *From giant planets to cool stars*, M. Marley, ed., 1999.
9. C. Goukenleuque, "Radiative equilibrium model of 51 Peg," in *From giant planets to cool stars*, M. Marley, ed., 1999.
10. S. Seager and D. D. Sasselov, "Extrasolar giant planets under strong stellar irradiation," *Ap. J. Letters* **502**, pp. 157–160, 1998.
11. F. Allard, P. H. Hauschildt, I. Baraffe, and G. Chabrier, "Synthetic spectra and mass determination of the brown dwarf Gliese 229B," *Ap. J. Letters* **465**, pp. 123–127, 1996.
12. A. Burrows, M. Marley, W. B. Hubbard, J. I. Lunine, T. Guillot, D. Saumon, R. Freedman, D. Sudarsky, and C. Sharp, "A nongray theory of extrasolar giant planets and brown dwarfs," *Ap. J.* **491**, pp. 856–875, 1997.